Applied Clay Science 211 (2021) 106193

Contents lists available at ScienceDirect

Applied Clay Science

journal homepage: www.elsevier.com/locate/clay

Research Paper

Modelling of solute transport and microbial activity in diffusion cells simulating a bentonite barrier of a spent nuclear fuel repository

Mirjam Kiczka [a,*], Marek Pekala [a,1], Susanna Maanoja [b,c], Eveliina Muuri [c], Paul Wersin [a]

[a] University of Bern, Institute of Geological Sciences, Rock-Water Interaction, Baltzerstrasse 1+3, 3012 Bern, Switzerland
[b] Tampere University, Faculty of Engineering and Natural Sciences, Research group of Bio and Circular Economy, P.O. Box 541, 33014 Tampere, Finland
[c] Posiva Oy, Olkiluoto, 27160 Eurajoki, Finland

ARTICLE INFO

Keywords:
Reactive transport modelling
Sulfide
Organic matter
Engineered barrier system
Buffer-host rock interface
Geological disposal

ABSTRACT

Microbial sulfate reduction possesses a potential risk for the long-term safety of spent nuclear fuel repositories because under expected repository conditions sulfide is the main corroding agent for copper and copper-coated steel canisters foreseen in the Scandinavian disposal concepts. It is thus essential to understand and quantify the processes and factors impacting microbial sulfide production within and around compacted bentonite, which is planned to be used as a buffer material in many repository concepts. In the present study reactive transport modelling was applied to increase the understanding of diffusion cell experiments, which brought sand layers with or without inoculated microorganisms in contact with compacted and saturated bentonites of different mineralogy. Model results obtained for a sodium bentonite from Wyoming and a calcium bentonite from Bulgaria gave strong evidence for the activation of bentonite indigenous microorganisms, at least in zones of a reduced density close to the bentonite/sand interface. For all experiments, the calculations indicated that after an initial phase of favourable conditions, microbial activity was limited by the (bio-)availability of organic carbon. In the Bulgarian bentonite, characterized by a very low gypsum content, the model furthermore suggested some intermediate control of microbial sulfate reduction by sulfate availability. The present study thus demonstrated the rapid evolution of a transport limited system in settings where zones of microbial activity are in contact with highly compacted microbially-inactive bentonite. Gypsum dissolution calculated and determined experimentally for the Wyoming bentonite indicated significant gypsum dissolution in the first 2 cm from the interface during 450 days. The reactive transport model applied successfully in this study for the description of an experimental system followed the conceptual models for microbial sulfate reduction in repository settings. The results obtained offer insights regarding the mechanism and magnitude of biogeochemical reactions that might occur in the vicinity of the bentonite buffer surrounding the waste canister and in so doing, may be relevant for the near field of HLW repositories.

1. Introduction

The Scandinavian concept for the disposal of spent nuclear fuel (SNF) in a deep geological repository foresees the construction of an engineered barrier system (EBS) in crystalline host rock (Posiva, 2018; SKB, 2010a). In the disposal concept, the SNF will be encased in copper canisters, which are emplaced in vertical deposition holes excavated in horizontal deposition tunnels. Compacted bentonite will be used as buffer material surrounding the canisters in the deposition holes and as backfill material of the deposition tunnels. The bentonite barriers play a central role for the long-term safety of the repository, because they isolate the canisters from flowing groundwater, protect them from corrosive agents (e.g. sulfide), shield them from detrimental mechanical processes and retard migration of radionuclides released in case of canister failure (Posiva, 2018; SKB, 2010a).

However, bentonite may also be a source of nutrients for microorganisms. Although microbial activity will largely be suppressed within highly compacted bentonite (Bengtsson and Pedersen, 2017), it might evolve in the excavated damaged zone (EDZ) at the bentonite – rock interface (Stroes-Gascoyne, 2010; Stroes-Gascoyne et al., 2011). Of

* Corresponding author.
E-mail address: mirjam.kiczka@geo.unibe.ch (M. Kiczka).
[1] present address: Federal Office for the Safety of Nuclear Waste Management (Bundesamt für die Sicherheit der nuklearen Entsorgung – BASE), 11,513 Berlin, Germany.

https://doi.org/10.1016/j.clay.2021.106193
Received 26 March 2021; Received in revised form 4 June 2021; Accepted 12 June 2021
Available online 23 June 2021

particular concern for long-term safety are sulfate-reducing microorganisms (SRM) that, by using organic matter (OM) or H_2 as an electron donor and sulfate as an electron acceptor, release sulfide to the system, which is the primary corrosive species for copper (King et al., 2013). The flux of sulfide in the bentonite barrier towards the canister thus exhibits the major control on corrosion and integrity of the canister (King et al., 2017).

Hence, various studies quantified the release and flux of sulfide and ensuing corrosion of copper canisters in deep geological repositories, using methods from simplified mass balance and transport considerations (Briggs et al., 2017; SKB, 2010b; Werme et al., 1992) to elaborated reactive transport calculations (Cloet et al., 2017; King et al., 2020; Pekala et al., 2019a; Pekala et al., 2020; Pekala et al., 2019b; Wersin et al., 2014). Depending on the complexity of the models, assumptions regarding the parameterization of the microbial sulfate reduction and the availability of nutrients, i.e. sulfate and OM are required. Microbial sulfate reduction kinetics were extracted either from experimental studies with simplified organic molecules (Hallbeck, 2014; Maia et al., 2016) or from natural analogue studies (Glombitza et al., 2013; Holmer and Storkholm, 2001). The mobility and bioavailability of OM in bentonite was shown to be limited due to its recalcitrant nature (Marshall et al., 2015). Based on this finding, some reactive transport studies considered a fraction of 1 to 10% of the total OM to be available for microbial sulfate reduction (King et al., 2020; Pekala et al., 2019a), whereas other studies accounted for the large uncertainty still associated with this parameter by conservatively assuming a bioavailability of 100% (Cloet et al., 2017; Pekala et al., 2020; Pekala et al., 2019b).

Recently, Maanoja et al. (2020) presented an experimental study to shed more light on the question, whether OM can dissolve from compacted bentonite and sustain biological sulfate reduction in an excavation-damaged zone (EDZ). In their study, the EDZ was simulated by diffusion cells with compacted bentonite (dry density ~ 1.35 g/cm^3) and a quartz sand layer . Three bentonites were studied, including two sodium bentonites originating from Wyoming and India and a calcium bentonite from Bulgaria. For each bentonite, one cell was prepared with the sand layer inoculated with known SRM communities, and a second one with sterilized sand (referred to as “uninoculated” cell). As a novelty to earlier studies (Bengtsson and Pedersen, 2016, 2017), no artificial OM source was added to the experiments by Maanoja et al. (2020). The authors presented several lines of evidence, e.g. Fe sulfide precipitation and the different evolution of key parameters (sulfate, dissolved inorganic and organic carbon) in the sand layers of inoculated and uninoculated cells that showed that OM dissolving from compacted bentonite can sustain the growth of microorganisms, including SRM. It was further concluded by Maanoja et al. (2020) that part of the microbial activity in the cell experiments presumably occurred in the bentonite, supporting the observation of viable sulfate reducing bacteria in commercial bentonites (Masurat et al., 2010; Matschiavelli et al., 2019).

While the data presented and interpreted by Maanoja et al. (2020) focused on the microbiology and OM in the sand layers, additional understanding of sulfur cycling in deep geological repository settings can be obtained from the data of this unique experimental set-up. In the present study, reactive transport modelling was used as a tool to unravel and quantify the main coupled geochemical processes in the experiments, providing insights into controls of microbial activity in different bentonites and their evolution over time, as well as providing constraints for the bioavailability of OM in bentonites. Additional experimental data on sulfur re-distribution in the interface region are presented, which support the model calculations and give evidence for gypsum dissolution and Fe-sulfide precipitation within the bentonites. A comprehensive picture of the major processes of nutrient release, solute transport and microbial activity in the experimental system was established, which improves the process understanding of sulfide production in zones of lower density at bentonite – rock interfaces.

2. Materials and methods

2.1. Experimental set-up and operation

The experimental set-up and sampling procedures were described in detail in Maanoja et al. (2020). Briefly, individual diffusion cells were prepared, each with two cylindrical sections, one of 16 cm height and 20 cm diameter with saturated compacted bentonite and one of 4.3 cm height and 16 cm diameter with loosely packed quartz sand (Fig. 1). Both compartments were separated by a titanium filter. The present study focussed on the sodium-rich bentonite from Wyoming and the calcium-rich bentonite from Bulgaria (Table 1). While the Wyoming bentonite sample was characterized by a high montmorillonite content of 88 mass-% and a gypsum inventory of 0.12 mass-% S-SO_4, the Bulgarian bentonite sample had almost 20% less montmorillonite (70 mass-%) and contained very little gypsum, amounting to less than 0.05 mass-% S-SO_4 (Kiviranta and Kumpulainen, 2011; Kumpulainen et al., 2016; Maanoja et al., 2020). For each bentonite, two cells were prepared, one with the sand layer inoculated with a mixture of known SRM and microorganisms enriched from groundwater of the finish repository site, in the following referred to as “inoculated cells” and another cell without any initial inoculation of the sand. In these latter “uninoculated cells”, however, microorganisms indigenous to the bentonites were present, because unlike the sand, the bentonite was not sterilized.

Artificial groundwater (AGW) of saline type (Hellä et al., 2014) was used to saturate the bentonite, which was compacted to a target dry density of 1400 kg/m^3. Due to swelling in the homogenization phase and once in the experimental phase, due to breaking of plunger height-adapters, two re-compaction steps were required and final dry densities of 1314 to 1368 kg/m^3 were reached in the different cells. The impact of the re-compaction events on the sulfate and DOC content of the bentonites was however considered minor (<0.2%) (Maanoja et al., 2020). The entire set-up of the diffusion cells, including the initial bentonite and AGW, were de-oxygenated, assembled in a glovebox and sealed against atmosphere. After assembling the cells, the sand layer was saturated with the AGW using the sampling ports.

Every third week, approximately 3 vol-% of the porewater in the sand layer were extracted for analyses and simultaneously replenished by the same amount of fresh AGW. Some deviations from the sampling protocol were required as detailed in Maanoja et al. (2020). After 398 to 454 days, the cells were opened and four blocks, including the filter were cut from the central part of the bentonite, which had been in contact with the sand layer. The samples were sealed in several layers of vacuum foil and stored at 4°C until further processing.

Part of the bentonite samples were subjected to a sequential leaching in order to determine the remaining leachable sulfate content after the experiment. The sequential leaching method was outlined in detail in Maanoja et al. (2021) and is briefly summarized in the supplementary material (available online only).

2.2. Analytical techniques

The solutions of the regular sampling from the cell sand layers were analysed for pH, Eh, DIC, DOC, CH_4, sulfide, sulfate and total Fe as described in Maanoja et al. (2020). In addition, Cl concentrations were measured via ion chromatography (Dionex ICS-1600; SFS-EN ISO 10304) with an IonPac AS22 4×250 mm column, an ASRS 300, 4 mm suppressor at 31 mA and 4.5 mM Na_2CO_3/1.4 mM $NaHCO_3$ as an eluent at 1.2 mL/min. Samples for cation analysis (Na, NH_4, K, Ca, Mg, Sr) were filtered (PET 0.45 μm) and stored at 4°C until measured by a Metrohm 850 Professional IC, equipped with a Metrohm Metrosep C4–150/4.0 separation column, a Metrosep C4 Guard/4.0 pre-column and an upstream Metrosep RP 2 Guard/3.5 column using a 1.7 mM HNO_3^- and 0.7 mM dipicolinic acid eluent solution.

Spatially resolved elemental distributions in the uppermost 4–5 cm of the bentonite profile were examined using Scanning Electron

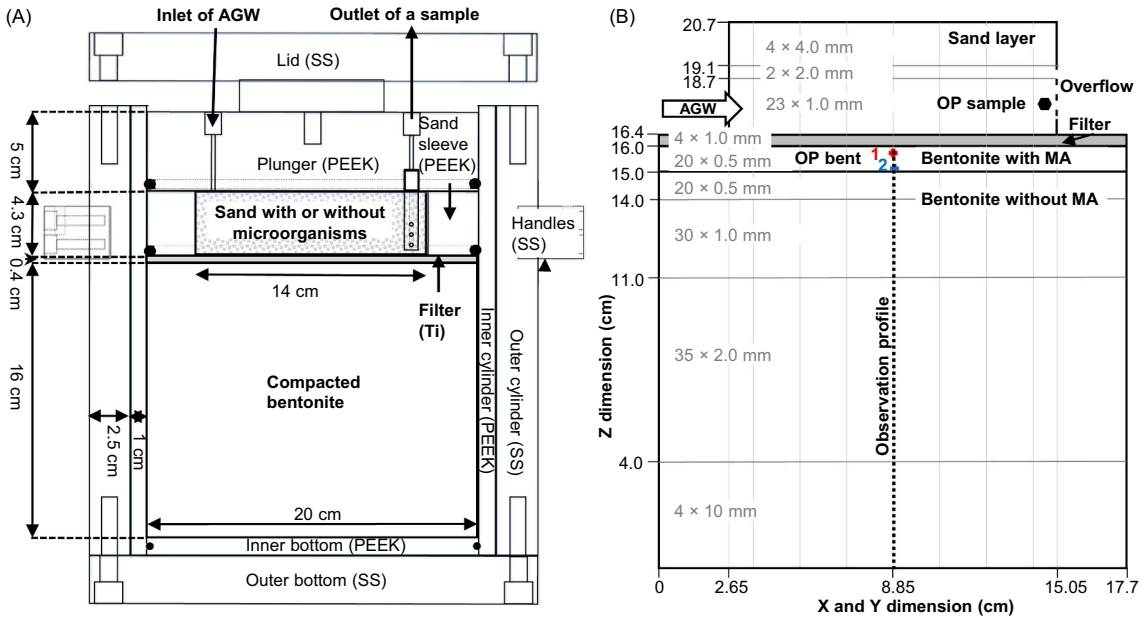

Fig. 1. Schematic slice plane of the cylindrical experimental cell (A) (modified after Maanoja et al. (2020); SS: stainless steel, PEEK: polyether ether ketone, Ti: titanium) and the cubic 3D model (B) with indication of the four domains (sand layer, filter, bentonite with microbial activity (MA) and bentonite without MA), observation points (OP) and inlet/overflow of artificial groundwater (AGW) during sampling events. Spatial discretization of the grid is indicated in grey. Horizontal lines subdivide the grid in regions with equal spatial resolution in Z dimension indicated by the number×size of the cells for each section. Spatial discretization is equal in X and Y dimension and visualized by the horizontal lines.

Microscopy (SEM) and Elemental Energy Dispersive Spectroscopy (SEM-EDX). Therefore, an approximately 1.5 cm thick and 5 cm long slice was cut from the central side of one bentonite block from each experiment, freeze dried, embedded in epoxy resin (Araldite) and polished. The analytical work was performed at a SEM (EVO-50 XVP, Carl Zeiss AG, Oberkochen, Germany) equipped with an EDAX Saphire light–element detector (AMATEK, Berwyn, Pennsylvania, USA). EDX element maps of 0.5×0.404 mm, a resolution of 128×100 pixels and a dwell time of 500 µs/pixel were acquired. The element maps were collected in a grid with 5 adjacent maps along the y-axis (parallel to the filter-bentonite interface) and 23–31 maps along the x-axis (distance to the interface). Distribution along the x-axis provided full coverage in the first few mm and 25–30% coverage of the following 4–5 cm. A total of 14 elements were probed and quantified without a standard as relative atom-% per map. The results for Fe and S are presented as "Al-normalized" chemical profiles, which describe the atomic ratio of Fe or S over Al as a function of the distance from the bentonite-filter interface. This approach is based on the assumption that from the elements probed Al is the least likely to vary along the profile with respect to quantity and localization (Hadi et al., 2019). In the profiles, each point with its error bars represents the average and range of the ratio of Fe or S over Al in the 5 maps at equal distance to the interface.

2.3. Reactive transport calculations

2.3.1. Conceptual model and main simplifications

The following conceptual model describes the main processes, which were considered relevant for the understanding and description of the evolution of porewater compositions and mineralogy in the experimental cells. It was built on conceptual models for microbial sulfate generation and transport in the near field of radioactive waste disposals described previously (Pekala et al., 2019a; Pekala et al., 2019b), but accounted for specific characteristics of the closed experimental system.

Solute transport in the cell experiments was assumed to be by diffusion only, except for sampling events, in which the injection of AGW induced an advective flow in the sand layer. Various experimental studies on diffusion in compacted bentonite indicated lower accessible porosities and thus effective diffusion coefficients for anions as compared to neutral species and cations (Glaus et al., 2017; Glaus et al., 2010; Muurinen et al., 2007; Van Loon et al., 2007). These observations led to the development of anion-exclusion models, which subdivided the porespace in bentonites into a "free" electrically neutral solution, a diffuse double layer (DDL) at the external surface of clay particles and an interlayer (IL) porespace. The IL porespace is generally considered devoid of any anions, due to the negative layer charge induced by isomorphic substitution (Appelo, 2013; Tournassat and Appelo, 2011; Wersin et al., 2004). For the implementation in the 3D reactive transport model, a simplification of the complex solute transport in bentonite matrixes was required. Thus, a simple Fickian diffusion model was used here, assigning the same diffusion coefficient to all dissolved species. Diffusion in the bentonite was assumed to take place only in the "free" porosity that is the fraction of the total porosity not affected by the surface charge of the clay minerals. All anions of the residual porewater and of the AGW, which was added to fully water saturate the sample, were considered to reside in this "free" porespace due to the anion exclusion effect.

It was assumed, that only a part of the OM of the bentonites could be released to the porewater and that dissolved OM was fully bioavailable and could simplistically be represented by the single generic model compound. The selected model compound $CH_2O(aq)$ can be considered representative for biodegradable DOC with respect to the average oxidation state of carbon and thus inherent reduction potential (Valle et al., 2018), although OM in porewaters obviously exhibits manifold compounds and variable carbon oxidation states, leading to a variety of stoichiometries in the sulfate reduction reaction (Liamleam and Annachhatre, 2007). Gypsum ($CaSO_4{\cdot}2H_2O(s)$) was taken to be the main source of sulfate in the system.

SRM were considered active in the sand layer of "inoculated" cells and in the top part of the bentonite in both, "inoculated" and "uninoculated" cells, where lower densities might have been favourable for the activation of indigenous microorganisms (Stroes-Gascoyne et al., 2011). In the model concept, the metabolism of SRM used sulfate as electron donor and DOC as electron acceptor, by this releasing sulfide and DIC to the porewater. It was further assumed that a Monod-type kinetic could

Table 1
Initial geochemical conditions used in the reactive transport modelling (RTM). Note, that for the bentonites only the "free" porosity is considered in the RTM. Mineralogy based on Kiviranta and Kumpulainen (2011) for Wyoming and Kumpulainen and Kiviranta (2015) for Bulgarian bentonite; *no data available, fitted; –§ minerals initially not present but allowed to precipitate. Composition of sand porewater largely follows the artificial groundwater (AGW) composition but accounts for some deviations measured in the porewater samples at day 0.

	Bentonite layer		Sand layer	
	Wyoming	Bulgarian	Wyoming	Bulgarian
Input initial porewater model				
Dry density (kg/m^3)	1355	1364	–	
Initial water content (%)	12.3	14.6	–	
Total porosity (–)	0.51	0.51	0.45	
"free" porosity (–)	0.09	0.16		
Chloride (mol/kg$_w$)	$1.35{\cdot}10^{-3}$	$1.35{\cdot}10^{-3}$		
CEC (cmol(+)/kg)	94.0	70.0		
Na^+ (cmol(+)/kg)	58.5	14.4		
Ca^{2+} (cmol(+)/kg)	24.5	46.2		
Mg^{2+} (cmol(+)/kg)	9.0	7.0		
K^+ (cmol(+)/kg)	2.0	2.5		
Transport				
D_e (m^2/s)	$2.3{\cdot}10^{-11}$	$4.1{\cdot}10^{-11}$	$3.0{\cdot}10^{-10}$	
Porosity (–)	0.09	0.16	0.45	
Mineralogy (mass-%)				
Montmorillonite (exchanger)	88.2	69.8		
Gypsum	0.9	0.035*	-§	
Calcite	0.2	11.0	-§	
Goethite	0.03	0.03	-§	
Quartz	3.9	10.6	100	
Siderite	–	0.1	-§	
Fe(II) source	0.05	0.05	–	
Mackinawite	-§	-§	-§	
Initial porewater / AGW composition				
pH	7.97	7.82	6.35	6.46
pe	−3.41	−6.03	–	–
Alk (eq/kg$_w$)	$5.6{\cdot}10^{-4}$	$1.5{\cdot}10^{-4}$	$5.1{\cdot}10^{-5}$	$5.6{\cdot}10^{-5}$
Ionic strength (mol/kg$_w$)	$5.9{\cdot}10^{-1}$	$4.5{\cdot}10^{-1}$	$2.0{\cdot}10^{-1}$	$2.1{\cdot}10^{-1}$
C_{inorg} (mol/kg$_w$)	$5.4{\cdot}10^{-4}$	$1.3{\cdot}10^{-4}$	$8.3{\cdot}10^{-5}$	$8.3{\cdot}10^{-5}$
S(VI) (mol/kg$_w$)	$9.8{\cdot}10^{-3}$	$1.4{\cdot}10^{-3}$	$2.1{\cdot}10^{-4}$	$2.7{\cdot}10^{-4}$
Cl (mol/kg$_w$)	$5.9{\cdot}10^{-1}$	$3.7{\cdot}10^{-1}$	$1.8{\cdot}10^{-1}$	$1.8{\cdot}10^{-1}$
Na (mol/kg$_w$)	$5.5{\cdot}10^{-1}$	$1.8{\cdot}10^{-1}$	$1.2{\cdot}10^{-1}$	$1.2{\cdot}10^{-1}$
K (mol/kg$_w$)	$4.7{\cdot}10^{-3}$	$7.0{\cdot}10^{-3}$	$3.1{\cdot}10^{-4}$	$3.7{\cdot}10^{-4}$
Ca (mol/kg$_w$)	$1.3{\cdot}10^{-2}$	$7.9{\cdot}10^{-2}$	$3.2{\cdot}10^{-2}$	$3.1{\cdot}10^{-2}$
Mg (mol/kg$_w$)	$1.4{\cdot}10^{-2}$	$1.6{\cdot}10^{-2}$	$2.7{\cdot}10^{-3}$	$2.7{\cdot}10^{-3}$
Fe (mol/kg$_w$)	$5.5{\cdot}10^{-7}$	$4.4{\cdot}10^{-4}$	$3.3{\cdot}10^{-7}$	$3.7{\cdot}10^{-7}$
S(II) (mol/kg$_w$)	–	–	–	–
Si (mol/kg$_w$)	$1.8{\cdot}10^{-4}$	$1.8{\cdot}10^{-4}$	$1.7{\cdot}10^{-4}$	$1.7{\cdot}10^{-4}$
log pCO_2	−3.69	−4.26	–	–

adequately describe the activity of SRM.

Sulfide was assumed to precipitate as mackinawite, with Fe(II) provided by a generic Fe(II) source. The simplification was chosen, because the available experimental data did not allow for a quantification of both, Fe(II) release by e.g. microbially induced Fe-oxide reduction, siderite dissolution or release from montmorillonite and the processes of sulfide immobilisation, including beside mackinawite precipitation also sulfidation of goethite and structural Fe(III) in montmorillonites. In particular, the natural variability in Fe content in the bentonite, limited data on sulfide fluxes and the activity of microorganisms and sulfide production in the bentonite itself impeded a detailed modelling of those processes.

2.3.2. Geochemical model and numerical implementation

For the reactive transport model the simulator PFLOTRAN (www.pflotran.org) was used (Hammond et al., 2014). Additional geochemical calculations, such as the determination of the initial porewater were performed with the computer code PhreeqC version 3.4.0 (Parkhurst and Appelo, 2013). The Andra/Thermochimie v.9b database was applied for all thermodynamic calculations (Giffaut et al., 2014; Grivé et al., 2015) considering a temperature of 25°C and utilizing the Lawrence Livermore National Laboratory (LLNL) parameterization of the extended Debye-Hückel aqueous activity model.

The geochemical model accounted for aqueous complexation and acid-base reactions of 12 primary species (H^+, O_2(aq), Na^+, Mg^{2+}, Ca^{2+}, K^+, Fe^{2+}, H_4SiO_4, Cl^-, CO_3^{2-}, SO_4^{2-}, S^{2-}) and 35 secondary species. Cation exchange reactions of Na^+, Ca^{2+}, Mg^{2+} and K^+ and surface site protonation/deprotonation at the clay-edge sites were included as equilibrium reactions according to the three-site model of Bradbury and Baeyens (1997). Calcite, gypsum, goethite, quartz and mackinawite dissolution and precipitation reactions were formulated as kinetic reactions but the rates were adjusted to approach local chemical equilibrium.

Gypsum dissolution and precipitation was implemented according to

$$CaSO_4{\cdot}2H_2O(s) \leftrightarrow Ca^{2+} + SO_4^{2-} + 2H_2O \quad (1)$$

The solid and dissolved OM pools were quantified in terms of organic carbon (OC). The leachable OC pool was treated as a mineral releasing CH_2O(aq) to the porewater according to

$$\text{Leachable OC}(s) \leftrightarrow CH_2O(aq) \quad (2)$$

Eq. (2) was implemented as a fast kinetic reaction to attain a constant CH_2O equilibrium concentration of 10^{-3} mol/L in the "free" porewater. This assumption was based on the observation that DOC concentrations in the sand layer of various experimental cells changed little over time (Maanoja et al., 2020) and that these concentrations were considered to be in diffusive equilibrium with the bentonite porewater.

The sulfate reduction reaction was considered to follow the stoichiometry of

$$2\,CH_2O(aq) + SO_4^{2-} + H^+ \rightarrow HS^- + 2H_2O + 2CO_2 \quad (3)$$

and implemented with a Monod kinetic reaction according to

$$R_{SRM} = k_{max}\left(\frac{[CH2O(aq)]}{[CH2O(aq)] + K^s_{CH2O(aq)}}\right)\cdot\left(\frac{[SO_4^{2-}]}{[SO_4^{2-}] + K^s_{SO_4^{2-}}}\right) \quad (4)$$

where R_{SRM} denotes the microbial sulfate reduction rate [mol/(L_{water}·s)], k_{max} is the maximum rate constant [mol/(L_{water}·s)], which could differ for sand and bentonite layers but remained constant over time, [CH_2O(aq)] and [SO_4^{2-}] are the concentrations of DOC, expressed as CH_2O, and sulfate in the porewater, respectively [mol/L_{water}] and $K^s_{CH2O(aq)}$ and $K^s_{SO_4^{2-}}$ are the half-saturation constants of CH_2O(aq) and sulfate, respectively [mol/L_{water}]. Half saturation constants were set to $K^s_{CH2O(aq)} = 5{\cdot}10^{-6}$ M CH_2O(aq) (Jin et al., 2013) and $K^s_{SO_4^{2-}} = 1{\cdot}10^{-5}$ M SO_4^{2-} (Nethe-Jaenchen and Thauer, 1984). The maximum rate constant k_{max} represents a fitting parameter and its parameterization is discussed in section 2.3.4.

The release of Fe(II) from the generic "Fe(II)_source" mineral was implemented as a fast kinetic reaction with an equilibrium constant K of 10^{-3} for the reaction

$$\text{Fe(II)\_source} \leftrightarrow \text{Fe(II)}(aq) \quad (5)$$

2.3.3. Discretization

The geometry of the experimental diffusion cells (Fig. 1A) were approximated using a structured rectangular grid with a 10 × 10 cell extension in the X-Y plane and 142 cells in the *Z*-dimension. Resolution in the Z dimension was variable with 0.5 mm in the first 2 cm of the bentonite next to the filter increasing to 1 cm at the bottom of the cells (Fig. 1B).

The model domain was divided into four internal regions based on material properties: the sand layer, the filter and the bentonite subdivided in a 1 cm thick region adjacent to the filter with microbial activity and a remaining region without microbial activity. The definition

of a 1 cm thick homogenous microbial active zone followed the spatial discretization during post-mortem investigations and the observation of lower dry densities closest to the filter (Maanoja et al., 2020). A more gradual distribution of active microbial communities due to small-scale density gradients could be envisaged but was beyond the scope of this work.

The standard simulation time covered a duration of 475 days. For the Wyoming models, the calculation time was extended to 6 years to follow the evolution of longer-term transients.

2.3.4. Parameterization of the initial conditions and calculation cases

Initial conditions in the bentonite were considered homogeneous over the entire bentonite domain and equal for experimental cells with the same bentonite (Table 1), except for the parameters relevant for the microbial sulfate reduction (Table 2).

For the Wyoming and Bulgarian bentonite, average dry densities of 1355 and 1364 kg/m^3, respectively were selected, based on the dry densities reported for individual cells and different stages of the experiment (Maanoja et al., 2020). The porosity distribution (interlayer, DDL and "free" porosity) in the bentonite was calculated using the structural clay model described in Wersin et al. (2016), which takes into account well-established crystallographic and electrostatic assumptions. A stacking number of 5, the interlayer spacing approximation according to Muurinen et al. (2007) and a Debye multiplier of 2 as proposed by Bolt and de Haan (1979) were applied. Note that the ionic strength of the "free" porewater solution as required for the calculation of the DDL thickness was not known a priori and thus, calculated porosity distribution and modelling of "free" porewater compositions were the result of an iterative process (Table 1).

A representative porosity of the sand layer of 0.45 was selected based on Maanoja et al. (2020). The porosity of the filter was estimated by scanning electron microscopy to be 0.1. Effective diffusion coefficients for solutes in the "free" porosity were scaled from a D_e for HTO at the dry density of interest of $1.3{\cdot}10^{-10}$ m^2/s (compilation of diffusion data in Kiczka et al. (2019)), resulting in D_e values for the "free" porosity of $2.3{\cdot}10^{-11}$ and $4.1{\cdot}10^{-11}$ m^2/s for the Wyoming and Bulgarian bentonite experiments, respectively. For the sand layer a D_e value of $3{\cdot}10^{-10}$ m^2/s was applied based on a tortuosity factor of 0.66 as suggested by Barnes and Turner (1998) for saturated sand. For the filter, a tortuosity of 0.1 and thus a D_e of $1{\cdot}10^{-11}$ m^2/s was chosen.

The initial "free" porewater composition was calculated with PhreeqC under the assumption of a closed system mixing of a residual porewater with the AGW. Note that in the PhreeqC simulation the residual porewater was assumed to be in equilibrium with atmospheric pCO_2 at a pH of 8 (Bradbury and Baeyens, 2003), whereas for the saturation of the bentonite carbonate free AGW was used (Maanoja et al., 2020). The Cl inventory of Wyoming bentonite of $1.35{\cdot}10^{-3}$ mol/kg dry bentonite (Bradbury and Baeyens, 2003), was adopted for the Bulgarian bentonite, due to the absence of analytical data. Residual and final "free" porewaters were taken to be in chemical equilibrium with calcite, quartz and goethite, and in the case of Bulgarian bentonite, also with siderite. Furthermore, the residual porewater was considered in chemical equilibrium with gypsum, whereas for the initial "free" porewater a gypsum undersaturation (SI of −1) was used to allow the Ca concentration in the initial porewater to be primarily controlled by the exchanger. For the Wyoming bentonite, the cation exchanger composition reported in Kiviranta and Kumpulainen (2011) was used to calculate the initial concentrations of Na^+, Mg^{2+} and K^+ in the initial porewaters, whereas for the Bulgarian bentonite, no data were available at the time of modelling and thus a Ca dominated exchanger composition was assumed as described in Table 1. However, the experimentally determined cation exchanger composition reported later by Maanoja et al. (2020) was close to the composition estimated here. The complete mineralogical composition of the bentonites as implemented in the reactive transport model is described in Table 1. For the Bulgarian bentonite, a very small gypsum pool of 0.035 mass-% was included, in line with a non-detectable gypsum content in bulk mineralogical investigations and a S-sulfate content of the bentonite, which can largely be attributed to barite (Kumpulainen and Kiviranta, 2015; Kumpulainen et al., 2016).

For each bentonite, three different modelling cases were distinguished, which differed with respect to the amount of the leachable OC and the microbial activity: i) an abiotic reference case, with no microbial activity (model w/o), ii) the uninoculated cell case, with microbial activity in the top first cm of the bentonite (model Unin) and iii) the inoculated cell case, with additional microbial activity in the sand layer (model Inoc) (Table 2).

The amount of the leachable organic carbon in the bentonites of the uninoculated cells was adopted from leaching experiments of untreated bentonite (Maanoja et al., 2021), whereas for the inoculated cells, a larger leachable OC pool was required to describe the data (Table 2). In the sand layer of all cells, an initial background DOC concentration of $5{\cdot}10^{-3}$ mol/L was used to account for an observed initial high concentration of DOC in this layer (Maanoja et al., 2020).

The maximum rate constant k_{max} of the microbial sulfate reduction reaction (eq. 4) was fitted to experimental DIC data in the early phase of the experiment, when neither DOC nor sulfate were considered limiting and the two Monod terms in eq. 4 approached 1. In a first step, the maximum rate constant k_{max} for the microbial activity of indigenous microorganisms in the bentonite of the uninoculated cell was fitted to the DIC evolution (model Unin). Because this was considered a bentonite intrinsic parameter, the same k_{max} constant was adopted for the microbial activity in the bentonite of the inoculated cell. In a second step, the k_{max} characterizing the microbial activity in the sand layer of the inoculated cells was fitted to the different evolution of DIC and sulfate in uninoculated and inoculated cells (Table 2).

3. Results and discussion

3.1. Diffusive transport

The measured evolution of Cl and Na concentrations in the sand layers of inoculated and uninoculated cells with the same bentonite were almost identical, demonstrating the comparability of both cells with respect to major geochemical and transport properties (Fig. 2). Between both bentonites, however, clear differences emerged, with higher Na and Cl concentrations in the Wyoming than in the Bulgarian bentonite cells. The Cl concentration breakthrough curves in the sand layer predicted by the reactive transport calculations match well the measured data of the temporal evolution and the final steady-state

Table 2
Parameterization of microbial sulfate reduction kinetics and related parameters in the different calculation cases for the reference case (w/o), the uninoculated (Unin) and inoculated (Inoc) cells. * leachable organic carbon pool based on independent leaching experiments of untreated bentonite (Maanoja et al., 2021). § increased leachable OC pool, required in model (Wyoming) or based on post-mortem leaching (Bulgarian).

	Wyoming			Bulgarian		
	w/o	Unin.	Inoc.	w/o	Unin.	Inoc.
Leachable OC pool (μg/g)	84.5*	84.5*	200§	163*	163*	300§
k_{max} bentonite in 1st cm (mol/(L_{water} s))	0	$3.0{\cdot}10^{-09}$	$3.0{\cdot}10^{-09}$	0	$7.0{\cdot}10^{-09}$	$7.0{\cdot}10^{-09}$
k_{max} sand (mol/(L_{water} s))	0	0	$9.0{\cdot}10^{-11}$	0	0	$1.0{\cdot}10^{-10}$

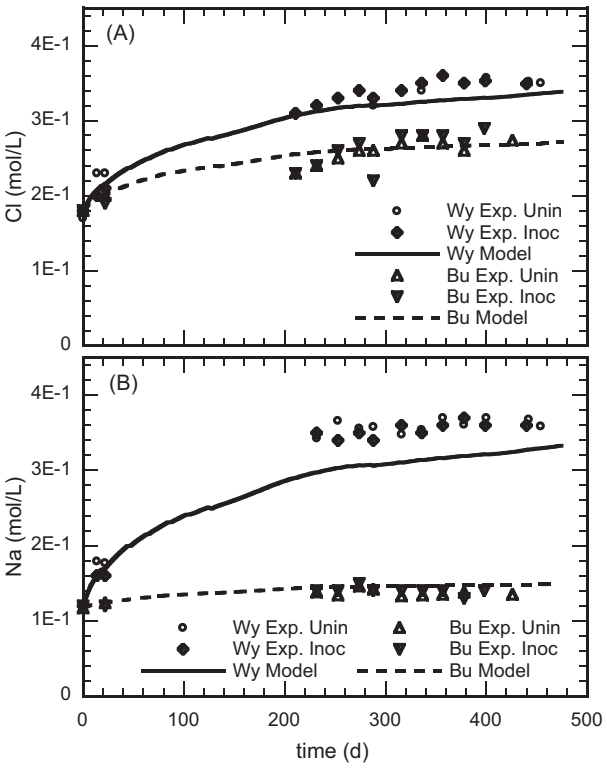

Fig. 2. Comparison of experimental (Exp.) and modelled Cl (A) and Na (B) concentrations at the sampling outlet of the sand layer (see Fig. 1) of the uninoculated (Unin) and inoculated (Inoc) cells with Wyoming (Wy) and Bulgarian (Bu) bentonite. Note that all three modelling cases for each bentonite plot closely together and thus only the model without any microbial activity is plotted for simplicity.

concentrations for both bentonites. Despite the same Cl inventories considered for the Wyoming and Bulgarian bentonite, an evolution towards higher Cl concentrations in the Wyoming cells was observed. This can be explained by the almost 20 mass-% lower montmorillonite content of the Bulgarian bentonite and, as a consequence, a larger anion accessible porosity of 0.16. Despite similar dry densities, the calculated anion accessible porosity of the Wyoming bentonite amounts to only 0.09 (Table 1). Thus, Cl concentrations in the bentonite porewater and the diffusivity of Cl in the experiment comply with the model assumptions that the Cl inventory was concentrated in the "free" porosity, due to the so called "anion exclusion" effect (Glaus et al., 2010; Van Loon et al., 2007; Wersin et al., 2004). Cl effective diffusion coefficients of $2.3{\cdot}10^{-11}$ and $4.1{\cdot}10^{-11}$ m^2/s as used in the model match the experimental data supporting previously reported anion diffusion coefficients in compacted bentonites and montmorillonites (Glaus et al., 2017; Glaus et al., 2010; Van Loon et al., 2007).

The evolution of Na concentrations reflected the difference between the Na- and Ca- bentonites in both the experiments and models. For the Wyoming bentonite, the model calculations underestimated the flux of Na to the sand layer. This could be due to uncertainties in the exchanger reactions or due to an oversimplified diffusion model. Cations are not restricted to the "free" porespace, but are thought to be also mobile in the interlayer and diffuse double layer, showing even larger effective diffusivities than water, an effect often referred to as "surface diffusion" (Appelo and Wersin, 2007; Gimmi and Kosakowski, 2011). For the Bulgarian bentonite, no information on the cation exchanger composition was available at the time of modelling and the selected Ca dominated composition yielded a good match of the experimental data (Fig. 2B; experimental data and model results for the evolution of Ca and Mg concentrations are provided in the supplementary material).

3.2. DIC evolution as a proxy for microbial activity

The calculated evolution of DIC in the sand layers for the three modelling cases showed distinct patterns, which were similar between the two bentonites (Fig. 3 top). The reference model, which only considered abiotic processes (model w/o), could not explain the DIC evolution in the sand layers as measured by Maanoja et al. (2020) for any of the four cells. It further indicated that DIC originating from the residual porewater and from calcite dissolution would account for less than 2 to 12% of the finally observed DIC concentrations in the sand layers. Adding microbial sulfate reduction in the bentonite only (model Unin) or in the bentonite and sand layer (model Inoc), a strong increase in the calculated DIC concentrations in the sand layer occurred and an adequate match of the measured DIC evolution in the four cell experiments was reached. Thus, the model calculations provided strong evidence for the activation of bentonite indigenous microorganisms at least in part of the bentonite layer as already postulated by Maanoja et al. (2020).

The evolution of DIC in the sand layer not only provided insight into microbial activity within the sand layer itself, but due to diffusive equilibration with the bentonite porewater also allowed to evaluate microbial activity taking place in the compacted bentonite. Based on the model calculations different phases of microbial activity could be distinguished.

The initial phase in all four cell experiments was characterized by a roughly linear increase of DIC lasting until day 250 / 300 and 100 / 190 in the uninoculated/inoculated cells of Wyoming and Bulgarian bentonite, respectively (Fig. 3 top panel). In this phase, sulfate and DOC in the sand and bentonite porewater were abundant and presumably not limiting bacterial activity. Hence, this linear increase of DIC was used to fit the maximum rate constant k_{max} of the Monod equation (eq. 4, Table 2) for the different model cases. For the Bulgarian bentonite a higher maximum rate constant and thus a faster initial sulfate reduction rate was determined compared to the Wyoming bentonite. This observation is in line with the ten times higher Most Probable Number (MPN) of SRM found in pristine Bulgarian bentonite compared to Wyoming bentonite (Maanoja et al., 2020). The k_{max} constants used in the model cases for the bentonite are in the upper range of maximum rate constants for microbial sulfate reduction reported for lake sediments (Holmer and Storkholm, 2001). The k_{max} values determined for the sand layers are in accordance with maximum rates determined for deep sediments (Glombitza et al., 2013).

It should be pointed out that the comparatively high rates required in the model calculations were partly due to the simplification used here, which allocated all DIC produced by microbial activity to a single microbial sulfate reduction reaction (eq. 3). Although various microbiological investigations of the sand and bentonite before and after the experiment provided strong evidence for the presence and activity of SRM and other microbial communities such as methanogens (Maanoja et al., 2020), a determination of the exact amount of SRM as part of the overall microbial community was not feasible. Thus, maximum sulfate reduction rates presented here can be considered conservative estimates and should be interpreted as potential reduction rates of SRM under conditions where DOC consumption by other microbial communities would be negligible. Nevertheless, this initial phase gave a clear indication of a rapid activation of added as well as bentonite indigenous microorganisms combined with favourable conditions in the early phase of the experiments.

After the initial phase of DIC concentrations increasing linearly, the DIC increase slowed down in both experimental data and model results (Fig. 3 top panel). In the final phase, experimentally determined DIC concentrations in the Bulgarian bentonite cells showed a decrease leading to an over-prediction of DIC concentrations by the model. In principal, the bend in the DIC curves could be due to an attained diffusive equilibration between bentonite and sand porewaters as seen in the evolution of Na and Cl (Fig. 2). This however would require

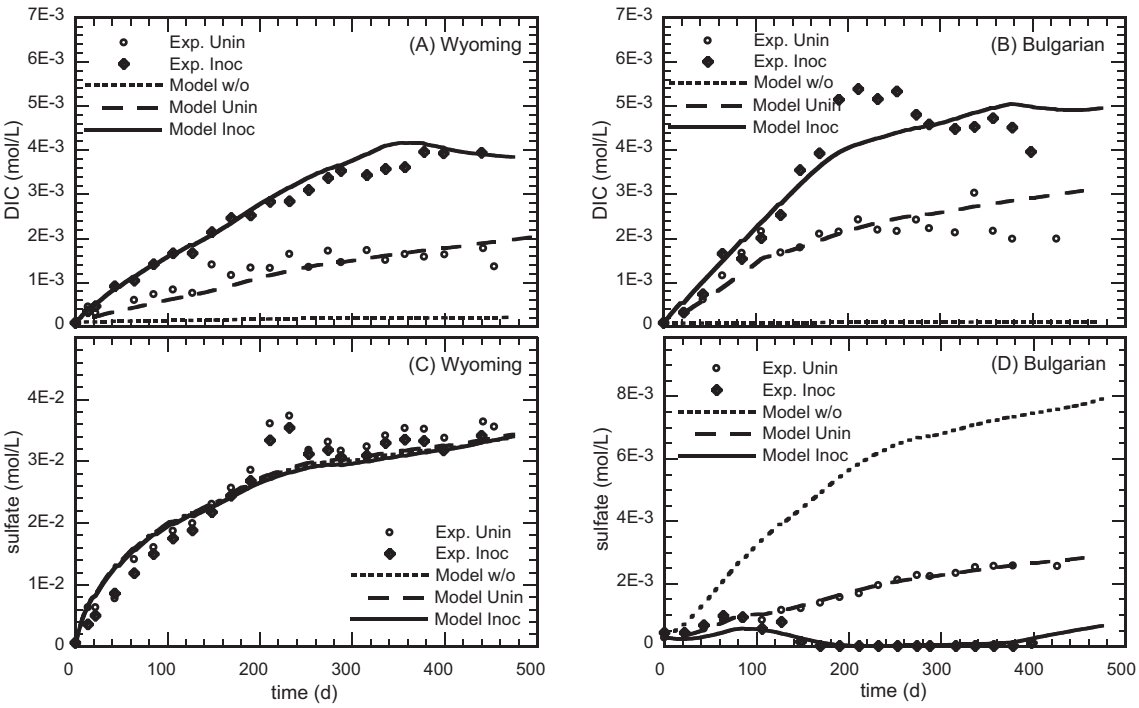

Fig. 3. Comparison of experimental and modelled dissolved inorganic carbon (DIC) (A,C) and sulfate (B, D) concentrations at the outlet of the sand layer. The Model w/o did not include microbial sulfate reduction (MSR), parameterization of the MSR in the Unin Model (MSR in bentonite only) and of the Inoc Model (MSR in bentonite and sand layer) according to Table 2. Note the different y-scales in Fig. C and D.

constant DIC concentrations in the bentonite porewater, which is not in line with DIC production by microbial activity.

3.3. Control of microbial activity by organic carbon availability

The model scenarios for the Wyoming bentonite predicted a complete depletion of the solid leachable organic carbon in the microbial active zone around day 160 and 350 in the uninoculated and inoculated cell, respectively. Due to ongoing microbial respiration, the depletion of the solid OC pool was reflected in the decrease of porewater DOC concentrations, which in turn slowed down the microbial sulfate reduction rate via the Monod term (eq. 4) (Fig. 4A,C). The reduction of

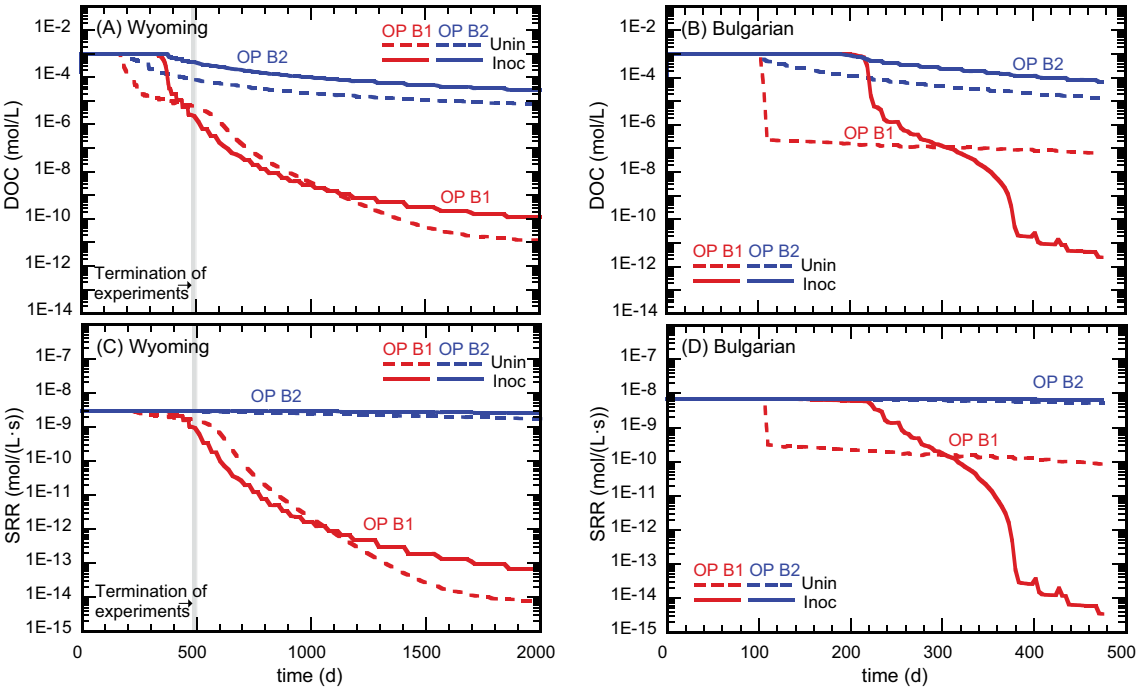

Fig. 4. Evolution of dissolved organic carbon (DOC) (top) and sulfate reduction rates (SRR) (bottom) calculated for two observation points (OP) in the microbial active zone of the bentonites of Wyoming (A, C) and Bulgarian (B, D) cells. OP B1 (red lines) is located close to the filter in 8 mm distance from the inactive bentonite, OP B2 (blue lines) is located 0.5 mm above the inactive bentonite. Note that in the left figures for Wyoming bentonite models, the calculation time was extended to ~six years. For reference to colours, the reader is referred to the web-version of this article.

microbial respiration in the bentonite eventually let to the bend in the DIC curve for the sand of the uninoculated cell around day 250 (Fig. 3A). The same pattern can be seen in the calculations of leachable OC and DOC of the Bulgarian bentonite, but with an earlier depletion of solid leachable OC and thus earlier decrease in microbial activity (Fig. 4B,D). The calculated relatively fast depletion of leachable OC despite a larger initial amount in the Bulgarian bentonite compared to the Wyoming bentonite can be explained by the higher microbial activity in the early stage of the experiment (Table 2). The predicted depletion of OC readily available for microbial respiration within the microbial active zone is in line with post-mortem observations of Maanoja et al. (2021), which showed a distinctly reduced amount of soluble OC in the first cm of the bentonite contacting the sand compared with bentonite in greater distance to the filter.

In principle, the predicted decrease in porewater DOC should at some stage be reflected in the measured sand layer DOC concentrations, in particular in the inoculated cells, where active microbes further consumed DOC in the sand layer. In the experiments, however, this was only observed in the late samples of the Bulgarian bentonite, but not in the Wyoming cell experiments (Maanoja et al., 2020). While this discrepancy might partly be due to uncertainties regarding the initial OC content of the sand layer, it might also be an indication for a limited bioavailability of the leachable organic carbon pool for the microbial community of the sand layer. Marshall et al. (2015) showed that long-chain aliphatic compounds, which are considered rather resistant to microbial degradation (Lorenz et al., 2007), prevailed in the water extractable OC of Wyoming bentonite. These might not have been available for the inoculated SRM, which only metabolize a relatively limited range of organic compounds, relying on precursor bacterial communities that break down complex organic matter by fermentation (Goldhaber, 2003).

Nevertheless, by reproducing the observed pattern of microbial activity, the model confirmed that using pools of leachable OC is an appropriate approximation for the readily bioavailable OC pool in bentonites. For the uninoculated cells, the leachable OC pools of 84.5 and 163 mg/kg for Wyoming and Bulgarian bentonite, respectively were determined independently in extensive leaching experiments of pristine bentonite (Maanoja et al., 2021). For the Wyoming bentonite this corresponds to around 6% of TOC (0.15 mass-%, reported by Kiviranta and Kumpulainen (2011)) and is thus well in line with water-extractable fractions of 6–8% of TOC determined for two Wyoming bentonites by Marshall et al. (2015).

For the inoculated cells, larger amounts of leachable OC were used in the model calculations. This was justified by post-mortem investigations, which showed an increased leachability of OC in the lower parts of the bentonite block (i.e. further away from the bentonite/sand interface) of inoculated cells compared with the same depth of uninoculated cells (Maanoja et al., 2021). Whether this different leachability of OC in inoculated and uninoculated cells was linked to variations in physical processing, such as compaction and squeezing or to the microbial activity in the sand layer remains unsolved so far. It should be pointed out that the leachable OC pools used in the calculations for the inoculated cells of 200 and 300 mg/kg for Wyoming and Bulgarian bentonite (Table 2), respectively, represent an approximation. The extent of the microbial active zone considered in the model had a direct impact on the calculated microbial sulfate reduction rates in the direct vicinity of the bentonite-sand interface once the solid leachable OC pool in the microbial active zone was depleted. The steep gradient in DOC and SRR rates within microbial active zones in the bentonite is visualized by the distinct evolution of both parameters at two observation points, OP B1 close to the filter in 8 mm distance to the inactive bentonite and OP B2 in 0.5 mm distance to the inactive bentonite (Fig. 4). At OP B2 DOC concentrations and thus sulfate reduction rates remained higher than at OP B1 further closer to the interface of the sand layer. This was accentuated in the prolonged calculation time for the Wyoming bentonite, indicating a shift of the diffusion front of DOC progressively deeper into the inactive bentonite zone and pointing to the final control of microbial activity by diffusive transport.

3.4. Control of microbial activity by sulfate availability

In the sand layer of the Wyoming bentonite cells measured sulfate concentrations increased up to almost $4{\cdot}10^{-2}$ mol/L, which was well matched by the model results (Fig. 3C). At these concentrations, microbial sulfate reduction should not be limited by sulfate availability in either the bentonite porewater or the sand layer of the Wyoming bentonite cells. The effect of microbial sulfate reduction on the sulfate concentration in the sand layer of the inoculated cell was small and calculated to be $9{\cdot}10^{-4}$ mol/L, which was close to the measured difference in sulfate and DIC concentrations of $2{\cdot}10^{-3}$ mol/L and $1–3{\cdot}10^{-3}$ mol/L, respectively.

An entirely different picture emerged for the experiments with the Bulgarian bentonite. Sulfate concentrations measured in the sand layers were not only approximately one order of magnitude lower than for the Wyoming bentonite but also showed entirely different patterns for the uninoculated and inoculated cell (Fig. 3D). The reactive transport calculations using the parameterization of Table 2 captured the magnitude of experimentally observed sulfate concentrations in the two cells and closely followed their evolution over time. In contrast, reference case calculations without any microbial activity suggested sulfate concentrations around 4 times higher than measured in the uninoculated cell (Fig. 3D). A closer look at the model results reveals that the observed sulfate evolution in the two Bulgarian bentonite cells can be traced back to changes in microbial activity controlled by a close interplay of sulfate and organic matter limitation.

The following timeline can be envisioned for the transient phases captured in the experiments with the Bulgarian bentonite (Fig. 5): Upon the onset of the experiment, the small amount of gypsum in the Bulgarian bentonite dissolved and higher sulfate concentrations in the porewater compared with the AGW in the sand layer induced a diffusion of sulfate from the bentonite to the sand layer in both cells. Microbial sulfate reduction in the interface region consumed part of the sulfate, indicated by the difference between the reference case and the two cases including microbial activity. Around day 75, the gypsum pool in the microbial active zone was depleted, and porewater sulfate concentrations in the bentonite porewaters decreased due to ongoing microbial sulfate reduction, thus leading to a bending of the curve of sulfate

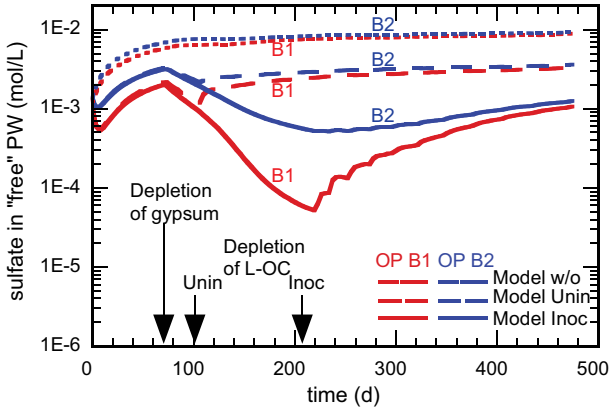

Fig. 5. Evolution of sulfate in the "free" porewater of the microbial active zone of the bentonite calculated with the three models for Bulgarian bentonite. The red and blue lines of the same signature indicate calculations for observation points (OP) B1 and B2 in 8 mm and 0.5 mm distance from the inactive bentonite, respectively, which corresponds to 2 mm (B1) and 9.5 mm (B2) distance from the bentonite-filter interface. Arrows indicate the time for which the models predict the depletion of the solid gypsum or leachable organic carbon (L-OC) pool in the microbial active zone. For reference to colours, the reader is referred to the web-version of this article.

evolution in the uninoculated cell experiment. In the inoculated cell, the onset of microbial sulfate reduction in the sand layer consumed the remaining in-diffusing sulfate and increased the DIC concentration in the sand layer (Fig. 3B). The depletion of the gypsum pool was closely followed by a depletion of the solid leachable OC in the microbial active bentonite zones around day 100 and 200 in the uninoculated cell and inoculated cell, respectively, leading to a rapid decrease in DOC in the microbial active zones (see section 3.3). Due to the limited availability of OC, microbial sulfate reduction in the bentonite slowed down, allowing for a recovery of sulfate concentrations by diffusion from deeper, microbially non-active layers. This was reflected in the resumption of increasing sulfate concentrations in the sand layer of the uninoculated cell (Fig. 3D). In the sand layer of the inoculated cell, microbial sulfate reduction rates were limited by the influx of sulfate. While the model suggested a gradual slowdown of microbial activity, the measured sudden decrease of DIC concentrations in the inoculated cell indicated a rather abrupt reduction in microbial activity during the experiment, maybe due to the inactivation of part of the microbial community. Such an inactivation was also indicated by post-mortem analyses of SRM genes and potential sulfate reduction rates showing, that a lot of the SRM cells in the inoculated sand of the Bulgarian cell were dormant (Maanoja et al., 2020).

3.5. Sulfur cycling

The diffusive flux of sulfate into the sand layer of the cells and the reduction of sulfate to sulfide by microbial sulfate reduction in the bentonite induced the dissolution of gypsum and a receding gypsum dissolution front over time. For the Wyoming experiments, a complete gypsum dissolution in the first few millimetre was calculated, which was followed by a sharp increase in gypsum content up to the operationally defined boundary of microbial active and inactive bentonite at 1 cm from the interface and a depletion of gypsum of >10% up to 3 cm from the interface (Fig. 6A). Differences between calculations for the inoculated and uninoculated case were only minor, as the models only differed with respect to the additional sulfate reduction in the sand layer enhancing slightly the concentration gradient between sand and bentonite porewater for the inoculated cell. The calculated depletion front is broadly in line with post-mortem leaching experiments indicating a sulfate (gypsum + dissolved sulfate) depletion front of around 2 cm (Fig. 6B). Sulfate released from the top cm corresponds to less than 20% of the sulfate released from the deeper layers. At depths greater than 2 cm, no significant variation was observed and differences between samples from the inoculated and uninoculated cells were presumably due to natural inhomogeneities or analytical uncertainties rather than being induced by the inoculation of the sand layer. Similarly, a depletion front of 2 cm could be extracted from the spatially higher resolved S/Al profiles (Fig. 6C). In this upper zone, S/Al ratios were relatively constant, whereas at a greater distance to the interface, higher and in particular more variable S/Al ratio were determined. This could be attributed to the presence of larger individual gypsum grains in some of the mapped areas, which were absent in the zone close to the interface. In contrast to the model predictions for sulfate/gypsum and leachable sulfate of the leaching tests (Fig. 6A, B), the S/Al ratios did not exhibit a sharp gradient at the interface. This might be due to the fact, that SEM-EDX only detects elements but cannot reveal their valence state. Thus, the S/Al ratio captured both, sulfate and sulfide, which might either be pyrite present as accessory mineral or sulfide produced by microbial sulfate reduction and attenuated in the bentonite. Note, that the Wyoming bentonite had 0.15 mass-% of sulfidic S, which was in the same range as the sulfur initially bound to gypsum (0.11 mass-%) (Kiviranta and Kumpulainen, 2011), thus providing already a constant S/Al baseline. However, the absence of an interface gradient for the S/Al ratios might be taken as an indication for microbial sulfate reduction and immobilisation close to the zone of production. This was also indicated by the model calculations, suggesting significant proportions of secondary sulfides in the zone of microbial activity.

For the Bulgarian bentonite, model calculations (not shown) suggested that the small gypsum pool entirely dissolved over almost the entire bentonite profile and that the sulfur inventory close the interface was dominated by secondary sulfide species. Due to the low sulfate content, no reliable sulfate leaching data were available for a robust

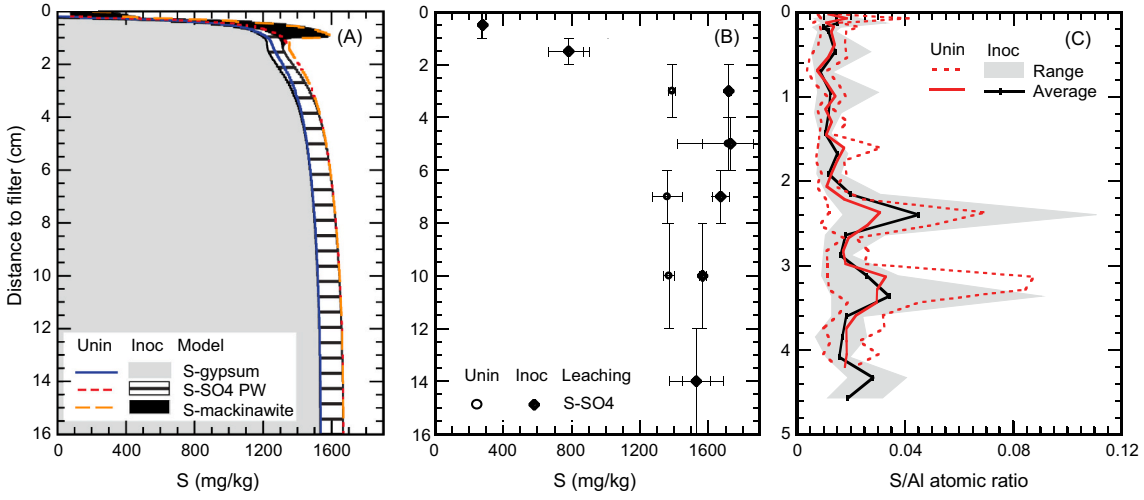

Fig. 6. Depth profiles of sulfur species in the Wyoming bentonite cells after termination of the experiment (A) as calculated by the models, note that both models are almost identical (filled areas representing the inoculated model scenario, the coloured lines the results for the uninoculated model); (B) as determined by sequential leaching experiments, with x-error bars indicating the range given by the 2 processed samples per depth and the vertical y-error bars indicating the sampling interval and (C) and S/Al atomic ratios as determined by post-mortem SEM-EDX. Note that the Wyoming bentonite contains 0.15 mass-% of S in pyrite, which is not included in the presented model results, but adds to the measured S/Al ratio in plot C. Plot A and B show the full bentonite profile, whereas for the S/Al ratios only the top 5 cm are shown. For reference to colours, the reader is referred to the web-version of this article.

comparison of model and experimental data. However, S/Al ratios exhibited a rather homogenous low ratio over the investigated area, with the exception of the inoculated cell profile, where S/Al ratio showed a sharp increase at the interface to the filter (Fig. S3 in supporting material). A parallel sharp increase in Fe/Al ratios provided a strong indication for precipitated FeS, which might either have formed due to microbial activity in the top layer/surface of the bentonite or back diffusion of S^{2-} produced in the sand layer.

For both bentonites, the model predicted significant local precipitation of FeS in the microbial active zone, which was not supported by the experimental S/Al profiles in that extent. Whether this is due to i) an overestimation of microbial sulfate reduction by the simplified formalism applied in the model calculations, ii) a presumably more gradually distributed microbial activity in the bentonites or iii) an underestimation of S^{2-} diffusion due to the modelled rapid FeS precipitation induced by the generic Fe(II)_source remains unsolved at present.

Despite these remaining uncertainties, combined experimental and model results strongly supported the hypothesised main processes of the sulfur cycle at bentonite-rock interfaces in repository settings. Moreover, the results confirmed the dissolution of gypsum as major sulfate source, the diffusion of sulfate according to concentration gradients from the higher sulfate containing porewater to areas of lower sulfate concentration, the reduction of sulfate by microbial sulfate reduction and the immobilisation of sulfide within the bentonite. In the present modelling exercise, this latter process was simplified as mackinawite precipitation. However, different processes recently investigated such as sulfidation of goethite or structural Fe(III) in montmorillonite (Pedersen et al., 2017; Svensson et al., 2017) may play a key role in the attenuation of sulfide in bentonite and should be further investigated and incorporated in future models.

4. Conclusions

Reactive transport calculations provided a valuable tool to improve the understanding of complex biogeochemical processes in the diffusion cell experiments of Maanoja et al. (2020), which investigated the role of organic carbon on microbial sulfate reduction in the context of a spent nuclear fuel repository. Different calculation scenarios gave strong evidence for the activation of bentonite indigenous microorganisms and favourable conditions for microbial sulfate reduction in the early phase of the experiments. Already in the short transient phase covered by the experiments, a shift from microbial activity only constrained by community size to a microbial activity limited by the availability of organic carbon was indicated. The comparison of two bentonites further underlined the importance of transport constraints and of variable availability of electron donors versus acceptors over time and space for the evolution of microbial sulfate reduction rates in excavated damaged zone (EDZ) surrounding the bentonite barrier and/or in zones of lower bentonite density within geological repositories.

The model, which closely followed those put forward in recent safety assessments, allowed an accurate representation of important experimental observations regarding solute transport, mineral reactions and microbial activity. By this, the results of the study supported common simplifications in performance assessment models in terms of selected processes, their mathematical representation and parameterisation and can be used to further decrease uncertainties in saftey assessments. However, given the extremely short experimental duration in comparison with the required life-time of a repository, some important questions for the extrapolation of microbial activity on the long-term remained. These include bacterial growth and decay, the effect of micronutrients (e.g. N, P), the role of alternative electron donors such as H_2 or the question of a threshold density of bentonite for microbial activity. Further research is also needed with respect the attenuation of sulfide in bentonite, both from an experimental and a modelling perspective.

Declaration of Competing Interest

The authors declare that they have no known competing financial interests or personal relationships that could have appeared to influence the work reported in this paper.

Acknowledgements

This work was funded by Posiva Oy. We thank B. Pastina, K. Koskinen and M. Vuorio for the planning and support of this project. L. Lehtinen, L. Salminen, K. Raassina, and R. Aalto from Tampere University and P. Bähler, C. Pichler, H.N. Waber, A. Jenni and A. Berger from University of Bern supported this project with laboratory and analytical work. We thank A. Nuottajärvi and M. Karttunen for their technical assistance in terminating the laboratory systems.

Appendix A. Supplementary data

Supplementary data to this article can be found online at https://doi.org/10.1016/j.clay.2021.106193.

References

Appelo, C.A.J., 2013. A Review of Porosity and Diffusion in Bentonite, Posiva Working Report 2013–29. Posiva Oy, p. 36.
Appelo, C.A.J., Wersin, P., 2007. Multicomponent Diffusion Modeling in Clay Systems with Application to the Diffusion of Tritium, Iodide, and Sodium in Opalinus Clay. Environ. Sci. Technol. 41, 5002–5007.
Barnes, C.J., Turner, J.V., 1998. Chapter 5 - Isotopic Exchange in Soil Water. In: Kendall, C., McDonnell, J.J. (Eds.), Isotope Tracers in Catchment Hydrology. Elsevier, Amsterdam, pp. 137–163.
Bengtsson, A., Pedersen, K., 2016. Microbial sulphate-reducing activity over load pressure and density in water saturated Boom Clay. Appl. Clay Sci. 132-133, 542–551.
Bengtsson, A., Pedersen, K., 2017. Microbial sulphide-producing activity in water saturated Wyoming MX-80, Asha and Calcigel bentonites at wet densities from 1500 to 2000kgm−3. Appl. Clay Sci. 137, 203–212.
Bolt, G.H., de Haan, F.A.M., 1979. Anion exclusion in soil. In: Bolt, G.H. (Ed.), Soil Chemistry B. Physico-Chemical Models. Elsevier, Amsterdam, pp. 233–257.
Bradbury, M.H., Baeyens, B., 1997. A mechanistic description of Ni and Zn sorption on Na-montmorillonite Part II: modelling. J. Contam. Hydrol. 27, 223–248.
Bradbury, M.H., Baeyens, B., 2003. Porewater chemistry in compacted re-saturated MX-80 bentonite. J. Contam. Hydrol. 61, 329–338.
Briggs, S., McKelvie, J., Keech, P., Sleep, B., Krol, M., 2017. Transient modelling of sulphide diffusion under conditions typical of a deep geological repository. Corros. Eng. Sci. Technol. 52, 200–203.
Cloet, V., Diomidis, N., Pekala, M., Wersin, P., Smith, P., 2017. An Evaluation of Sulphide Fluxes in the Near Field of a HLW Repository, Nagra Technical Report 17–04. Nagra, Wettingen, Switzerland.
Giffaut, E., Grivé, M., Blanc, P., Vieillard, P., Colàs, E., Gailhanou, H., Gaboreau, S., Marty, N., Madé, B., Duro, L., 2014. Andra thermodynamic database for performance assessment: ThermoChimie. Appl. Geochem. 49, 225–236.
Gimmi, T., Kosakowski, G., 2011. How Mobile are Sorbed Cations in Clays and Clay Rocks? Environ. Sci. Technol. 45, 1443–1449.
Glaus, M.A., Frick, S., Rossé, R., Van Loon, L.R., 2010. Comparative study of tracer diffusion of HTO, 22Na+ and 36Cl− in compacted kaolinite, illite and montmorillonite. Geochim. Cosmochim. Acta 74, 1999–2010.
Glaus, M.A., Frick, S., Van Loon, L.R., 2017. Diffusion of Selected Cations and Anions in Compacted Montmorillonite and Bentonite, Nagra Technical Report 17–12. Nagra, Wettingen, Switzerland.
Glombitza, C., Stockhecke, M., Schubert, C., Vetter, A., Kallmeyer, J., 2013. Sulfate reduction controlled by organic matter availability in deep sediment cores from the saline, alkaline Lake Van (Eastern Anatolia, Turkey). Front. Microbiol. 4, 209.
Goldhaber, M.B., 2003. 7.10 - Sulfur-rich Sediments. In: Holland, H.D., Turekian, K.K. (Eds.), Treatise on Geochemistry. Pergamon, Oxford, pp. 257–288.
Grivé, M., Duro, L., Colàs, E., Giffaut, E., 2015. Thermodynamic data selection applied to radionuclides and chemotoxic elements: an overview of the ThermoChimie-TDB. Appl. Geochem. 55, 85–94.
Hadi, J., Wersin, P., Serneels, V., Greneche, J.-M., 2019. Eighteen years of steel–bentonite interaction in the FEBEX in situ test at the Grimsel Test Site in Switzerland. Clay Clay Miner. 67, 111–131.
Hallbeck, L., 2014. Determination of sulphide production rates in laboratory cultures of the sulphate reducing bacterium Desulfovibrio aespoeensis with lactate and H2 as energy sources. In: Technical Report TR-14-14, Svensk kärnbränslehantering AB. Swedish Nuclear Fuel and Waste Management.
Hammond, G.E., Lichtner, P.C., Mills, R.T., 2014. Evaluating the performance of parallel subsurface simulators: an illustrative example with PFLOTRAN. Water Resour. Res. 50, 208–228.

Hellä, P., Pitkänen, P., Löfman, J., Partamies, S., Vuorinen, U., Wersin, P., 2014. Safety case for the disposal of spent nuclear fuel at Olkiluoto. Definition of Reference and Bounding Groundwaters, Buffer and Backfill Porewaters. Posiva Report. Vol. 2014-04. 164 pages. Posiva Oy, Olkiluoto.
Holmer, M., Storkholm, P., 2001. Sulphate reduction and Sulphur cycling in lake sediments: a review. Freshw. Biol. 46, 431–451.
Jin, Q., Roden, E.E., Giska, J.R., 2013. Geomicrobial Kinetics: Extrapolating Laboratory Studies to Natural Environments. Geomicrobiol J. 30, 173–185.
Kiczka, M., Pękala, M., Wersin, P., 2019. Radionuclide Solubility Limits and Migration Parameters for the Canister, Buffer and Buffer-Rock Interface for TURVA-2020, Posiva Working Report 2019-Xx. Posiva Oy, Olkiluoto, Finland.
King, F., Lilja, C., Vähänen, M., 2013. Progress in the understanding of the long-term corrosion behaviour of copper canisters. J. Nucl. Mater. 438, 228–237.
King, F., Chen, J., Qin, Z., Shoesmith, D., Lilja, C., 2017. Sulphide-transport control of the corrosion of copper canisters. Corros. Eng. Sci. Technol. 52, 210–216.
King, F., Kolar, M., Puigdomenech, I., Pitkänen, P., Lilja, C., 2020. Modeling microbial sulfate reduction and the consequences for corrosion of copper canisters. Mater. Corros. 72, 339–347.
Kiviranta, L., Kumpulainen, S., 2011. Quality Control and Characterization of Bentonite Materials, Posiva Working Report 2011–84. Posiva Oy, Olkiluoto.
Kumpulainen, S., Kiviranta, L., 2015. Technical Memo: Characterization of FISST-Candidate Materials, MEMO 9/2015–274. Helsinki, B+Tech.
Kumpulainen, S., Kiviranta, L., Karttunen, P., Keto, P., 2016. Composition and Properties of Alternative Buffer and Backfill Materials 2011–2015, Posiva Working Report 2016-XX. Posiva Oy, Olkiluoto.
Liamleam, W., Annachhatre, A.P., 2007. Electron donors for biological sulfate reduction. Biotechnol. Adv. $V 25, 452–463.
Lorenz, K., Lal, R., Preston, C.M., Nierop, K.G.J., 2007. Strengthening the soil organic carbon pool by increasing contributions from recalcitrant aliphatic bio(macro) molecules. Geoderma 142, 1–10.
Maanoja, S., Lakaniemi, A.-M., Lehtinen, L., Salminen, L., Auvinen, H., Kokko, M., Palmroth, M., Muuri, E., Rintala, J., 2020. Compacted bentonite as a source of substrates for sulfate-reducing microorganisms in a simulated excavation-damaged zone of a spent nuclear fuel repository. Appl. Clay Sci. 196, 105746.
Maanoja, S., Palmroth, M., Salminen, L., Lehtinen, L., Kokko, M., Lakaniemi, A.-M., Auvinen, H., Kiczka, M., Muuri, E., Rintala, J., 2021. The effect of compaction and microbial activity on quantity and release rate of water-soluble organic matter from bentonites. Appl. Clay Sci. https://doi.org/10.1016/j.clay.2021.106192. In this issue.
Maia, F., Puigdomenech, I., Molinero, J., 2016. Modelling rates of bacterial sulfide production using lactate and hydrogen as energy sources. In: Technical Report TR-16-05. Swedish Nuclear Fuel and Waste Management, Svensk Kärnbränslehantering AB.
Marshall, M.H.M., McKelvie, J.R., Simpson, A.J., Simpson, M.J., 2015. Characterization of natural organic matter in bentonite clays for potential use in deep geological repositories for used nuclear fuel. Appl. Geochem. 43–53.
Masurat, P., Eriksson, S., Pedersen, K., 2010. Evidence of indigenous sulphate-reducing bacteria in commercial Wyoming bentonite MX-80. Appl. Clay Sci. 47, 51–57.
Matschiavelli, N., Kluge, S., Podlech, C., Standhaft, D., Grathoff, G., Ikeda-Ohno, A., Warr, L.N., Chukharkina, A., Arnold, T., Cherkouk, A., 2019. The Year-Long Development of Microorganisms in Uncompacted Bavarian Bentonite Slurries at 30 and 60°C. Environ. Sci. Technol. 53, 10514–10524.
Muurinen, A., Karnland, O., Lehikoinen, J., 2007. Effect of homogenization on the microstructure and exclusion of chloride in compacted bentonite. Physics and Chemistry of the Earth, Parts A/B/C 32, 485–490.
Nethe-Jaenchen, R., Thauer, R.K., 1984. Growth yields and saturation constant of Desulfovibrio vulgaris in chemostat culture. Arch. Microbiol. 137, 236–240.
Parkhurst, D.L., Appelo, C.A.J., 2013. Description of input and examples for PHREEQC Version 3—A computer program for speciation, batch-reaction, one-dimensional transport, and inverse geochemical calculations. In: Chapter 43 of Section a, Groundwater Book 6. Modeling Techniques. U.S. Department of the Interior. U.S. Geological Survey.
Pedersen, K., Bengtsson, A., Blom, A., Johansson, L., Taborowski, T., 2017. Mobility and reactivity of sulphide in bentonite clays – Implications for engineered bentonite barriers in geological repositories for radioactive wastes. Appl. Clay Sci. 146, 495–502.
Pekala, M., Alt-Epping, P., Wersin, P., 2019a. 3D and 1D Dual-Porosity Reactive Transport Simulations - Model Improvements, Sensitivity Analyses, and Results from the Integrated Sulfide Project Inter-Model Comparison. Posiva Working Report 2018–31, Olkiluoto.
Pekala, M., Wersin, P., Cloet, V., Diomidis, N., 2019b. Reactive transport calculations to evaluate sulphide fluxes in the near-field of a SF/HLW repository in the Opalinus Clay. Appl. Geochem. 100, 169–180.
Pekala, M., Smith, P., Wersin, P., Diomidis, N., Cloet, V., 2020. Comparison of models to evaluate microbial sulphide generation and transport in the near field of a SF/HLW repository in Opalinus Clay. J. Contam. Hydrol. 228.
Posiva, 2018. Design and Production of the KBS-3H Repository, POSIVA 2016–10. Posiva Oy, Olkiluoto, Finland, p. 108.
SKB, 2010a. Design and Production of the KBS-3 Repository, SKB TR-10-12, Updated 2013–10. Stockholm, Sweden.
SKB, 2010b. Corrosion calculations report for the safety assessment SR-Site, SKB TR-10-66.
Stroes-Gascoyne, S., 2010. Microbial occurrence in bentonite-based buffer, backfill and sealing materials from large-scale experiments at AECL's Underground Research Laboratory. Appl. Clay Sci. 47, 36–42.
Stroes-Gascoyne, S., Hamon, C.J., Maak, P., 2011. Limits to the use of highly compacted bentonite as a deterrent for microbiologically influenced corrosion in a nuclear fuel waste repository. Phys. Chem. Earth 36, 1630–1638.
Svensson, D., Lundgren, C., Wikberg, P., 2017. Experiments with bentonite and sulphide – results from experiments 2013–2016, SKB P-16-31 (Svensk Kärnbränslehantering AB).
Tournassat, C., Appelo, C.A.J., 2011. Modelling approaches for anion-exclusion in compacted Na-bentonite. Geochim. Cosmochim. Acta 75, 3698–3710.
Valle, J., Gonsior, M., Harir, M., Enrich-Prast, A., Schmitt-Kopplin, P., Bastviken, D., Conrad, R., Hertkorn, N., 2018. Extensive processing of sediment pore water dissolved organic matter during anoxic incubation as observed by high-field mass spectrometry (FTICR-MS). Water Res. 129, 252–263.
Van Loon, L.R., Glaus, M.A., Müller, W., 2007. Anion exclusion effects in compacted bentonites: Towards a better understanding of anion diffusion. Appl. Geochem. 22, 2536–2552.
Werme, L., Sellin, P., Kjellbert, N., 1992. Copper canisters for nuclear high level waste disposal Corrosion aspects, SKB-TR-92-26. Sweden, p. 29.
Wersin, P., Curti, E., Appelo, C.A.J., 2004. Modelling bentonite–water interactions at high solid/liquid ratios: swelling and diffuse double layer effects. Appl. Clay Sci. 26, 249–257.
Wersin, P., Alt-Epping, P., Pitkänen, P., 2014. Sulphide Fluxes and Concentrations in the Spent Nuclear Fuel Repository at Olkiluoto. Posiva Oy.
Wersin, P., Kiczka, M., Koskinen, K., 2016. Porewater chemistry in compacted bentonite: Application to the engineered buffer barrier at the Olkiluoto site. Appl. Geochem. 74, 165–175.